Proceedings of the International Gas Turbine Congress 2003 Tokyo
November 2-7, 2003

IGTC2003Tokyo OS-101

Aerothermal Optimization of Micro-gasturbine Compressor Including Heat Transfer

R.A. Van den Braembussche , A.A. Işlek, Z. Alsalihi

Turbomachinery and propulsion Department
von Karman Institute for Fluid Dynamics
Waterloose steenweg, 72, B-1640, Sint-Genesius-Rode, BELGIUM
Phone: +32-2-359 96 09, FAX: +32-2-359 96 00, E-mail: vdb@vki.ac.be

ABSTRACT

The aerodynamic design and performance prediction of a two-dimensional compressor for a micro-gas-turbine application is described. Because of the uncommon geometry (2D with large relative clearance) and particular operating conditions (low Reynolds number with large heat transfer) one has first evaluated and calibrated the one-dimensional design and off-design performance prediction method by comparing predictions with those obtained from a three-dimensional Navier Stokes solver. It is shown that only minor modifications are required to reach a good agreement, once the impact on performance and flow conditions of the heat transfer at different location between inlet and outlet is evaluated.

A first optimization of the overall compressor geometry, in terms of range and performance, by means of the one-dimensional prediction model, is followed by a detailed impeller design. This is done by means of the VKI optimization system, based on an Artificial Neural Networks, a Database, Genetic Algorithm and three-dimensional Navier Stokes solver. Less than 30 iterations have been required to find the optimum geometry.

The design is completed by the definition of the optimum vaned diffuser geometry and an evaluation of the performance at 1/10 scaled button size compressor.

NOMENCLATURE

b	impeller width, blade height
Cp	specific heat
H	enthalpy
DR	diffusion ratio (W_{LE}/W_{SEP})
HNU	wake over jet velocity ratio (W_W/W_J)
M	Mach number
$\dot{m}$	mass flow
P	pressure
R	radius
R_G	gas constant
RPM	rotations per minute
T	temperature
u	non-dimensional meridional contour length
W	velocity
β	relative flow angle, blade angle (from meridional)
η	efficiency
μ	viscosity
π	pressure ratio
ρ	density
σ	slip factor

Subscripts

AD	adiabatic
J	jet
LE	leading edge
req	required, desired
SEP	separation
TE	trailing edge
TS	total to static
TT	total to total
W	wake
m	meridional

Superscripts

o	stagnation condition

Manuscript Received on April 24, 2003

INTRODUCTION

The search for more compact micro power sources to replace the heavy and large batteries, together with the developments of MEMS (Micro Electro Mechanical Systems) have stimulated the research in micro gasturbines in the last decade. The problems however are the very small dimensions and manufacturing constraints that make it more difficult to achieve the component performance required by the gasturbine cycle.

The Reynolds number, based on hydraulic diameter, can be as low as 5000. , suggesting laminar flow for the smallest samples. It is also unclear how much impact the relatively large surface roughness will have on boundary layer transition. The limitation of maximum RPM and the pressure ratio required for optimum cycle efficiency results in a non-optimum value for the non-dimensional specific speed. Manufacturing techniques and cost may limit the compressor and turbine geometry to two-dimensional which, for the high required pressure ratio, is not considered as an optimum configuration. Some mechanical dimensions such as clearance can not be scaled by the same ratio as the other ones and further increase the difficulty to reach a sufficiently high efficiency.

The temperature differences are the same as in larger gasturbines but occur over a distance that is an order of magnitude smaller. The resulting heat fluxes are therefore of the same order of magnitude as the energy involved in the compression and expansion.

As a consequence, the achievable performance needs to be verified and the design tools need to be adapted to these unconventional situation.

The goal of present paper is twofold:

- First to evaluate the accuracy of the existing aerodynamic design tools for micro gastubine components and introduce the modifications required for these applications.
- Secondly to use those methods for the design and optimization of a compressor at the typical conditions of this application and to quantify achievable performance.

The engine to be designed is a simple Brayton cycle gastubine with 260 W electric output. The principal design characteristics are listed in table 1.
Based on these data the compressor power is estimated at 2440 W and the Turbine power at 2700 W.
The heat transfer is estimated by Y. Ribaud (2002) at 500W to the compressor impeller, 100 W to the vaneless diffuser and 100W to the volute. The heat loss by the turbine impeller is estimated at 300 W. The difference between the turbine heat loss and compressor heat addition is the direct heating of the compressor by the combustion chamber.

Table 1 Design parameters

Compressor inlet pressure	Pa	101 300.
Compressor inlet temperature	^{o}K	288.
Compressor pressure ratio		2.75
Turbine inlet Temperature	^{o}K	1223.
Mass flow	gr./sec	12.5
RPM	/min	210 000.

COMPRESSOR DESIGN CONSIDERATIONS

The imposed limit on RPM in combination with the low volume flow and required pressure ratio result in a low specific speed impeller (NS = .253) and hence a large outlet over inlet radius ratio. Traditional radial compressors have an inlet over outlet section close to 1. This is normally achieved by a reduction of blade height from inlet to outlet. However low specific speed impellers have a small blade height and any reduction of the blade height towards the impeller exit would lead to extremely short blades and excessive clearance losses (Fig. 1). This means that the impeller outlet/inlet cross section area is proportional to the trailing- over leading edge radius ratio. Hence the diffusion required by present impellers is much larger than the conventional one and will lead to large separation zones and lower efficiency. Two dimensionality may also be a manufacturing requirement for very small impellers. The problem of large diffusion is further enhanced by the high pressure ratio of the impeller. The subsequent increase of density results in a proportional decrease of the volume flow at the impeller exit. The large outlet to inlet area ratio and the high density increase result in larger areas of separated flow at the impeller exit and lower the efficiency even more.
One way to limit the diffusion in the impeller is by increasing the tangential component of the relative velocity. One will therefore design the impeller with low inlet flow angles (β_{LE}) in combination with the maximum possible backward lean at the outlet (β_{TE}). This means that more pressure rise must be realized by the centrifugal forces and that a larger peripheral speed is required. However the latter one is limited by a maximum rotational speed of 210 000 RPM (because of bearing and dynamic problems) and a maximum impeller exit radius of 0.02 m (for mechanical reasons).
The increase of the impeller outlet temperature due to heat transfer increases the exit volume flow because, at constant pressure ratio, it lowers the density at impeller outlet ($\rho=P/R_GT$). Hence it reduces the diffusion and decreases separation in the 2D impeller.
A decrease of the inlet radius results in longer blades and flow channels in which a larger diffusion would be possible. However a smaller inlet radius means larger inlet velocity because the same mass flow has to pass a smaller inlet section with a larger blade blockage. It results in a proportional increase of required diffusion. There is anyway a minimum inlet radius to avoid that the axial part of the inlet section ($\pi.R_{LE}^2$) would become smaller than the inlet section at the leading edge ($2\pi.R_{LE}.b$) (FIG. 1). This would lead to an unacceptable deceleration of the absolute velocity at the impeller inlet. Minimum value of the inlet radius is limited to $.5*R_{TE}$. Typical values of the other dimensions are listed in table 3.

PRELIMINARY STUDY

It is not clear what performance can be expected with these uncommon geometries and what will be the impact of the large relative tip clearance values on performance. Taking into account the small blade height it may have a considerable effect.
One has therefore started to analyze a first geometry by means of a Navier-Stokes solver in order to quantify the effect of clearance and non-adiabatic flow on achievable performance. The detailed analysis of the flow is done by means of a Navier Stokes solver TRAF3D, developed by A Arnone (1994) at the university of Florence, Italy. Analyses have been made with the adiabatic version (wall temperature = local fluid temperature) and with the non adiabatic version with prescribed wall temperature ($TW=T_{wall}/T^{o}_{LE}$). In a first step this ratio was was defined in such a way that the resulting amount of heat transfer equals the prescribed value at the design point.

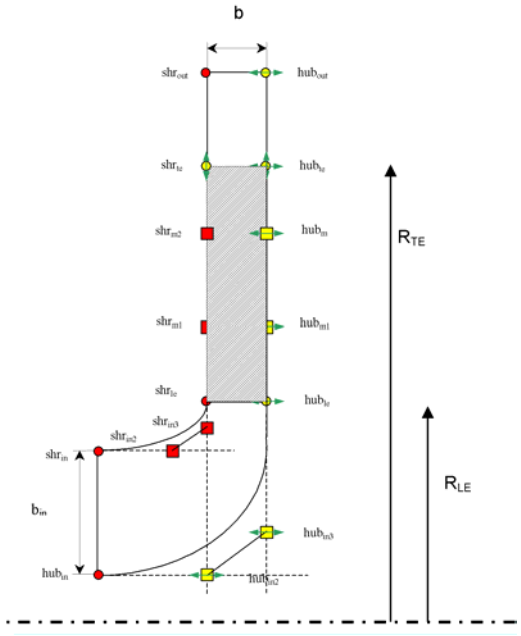

Fig. 1 Meridional cut of the 2D radial impeller

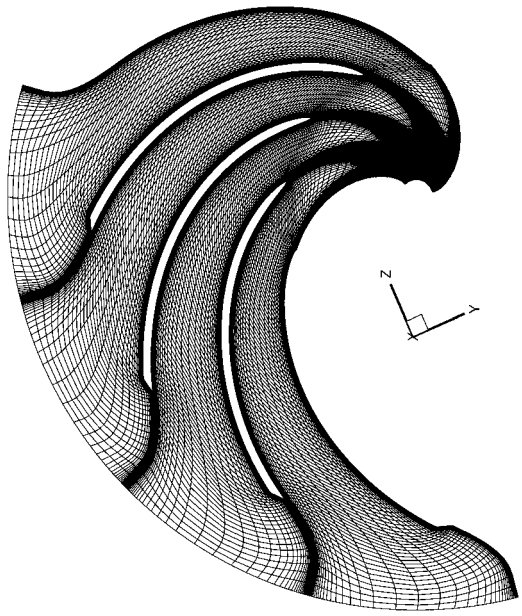

Fig. 2 Typical grid for the Navier Stokes calculations.

Results of these calculations will also be used for the verification of the predictions by the 1D program CCOD. A typical grid, used for the Navier Stokes calculations, is shown in figure 2. Calculations are limited to one channel (230 000. cells) extending downstream up to R/R_{TE} =1.1

Figure 3 and 4. show the impact of clearance and non adiabatic flow on the total to total efficiency and static over total pressure ratio.

A .1mm clearance with 1.7 mm blade height results in an efficiency drop of 5. to 10. points and a decrease of the pressure ratio by .3 over most of the operating range. The Navier Stokes solver also predicts a favorable effect of the clearance on range resulting on one side from a slight increase of the choking mass flow and on the other side from a considerable decrease of the surge mass flow. This decrease is attributed to a larger volume flow resulting from a lower pressure ratio.

The heat transfer results in a further decrease of the pressure ratio and a considerable decrease of the non adiabatic efficiency. A further shift of the surge limit to smaller mass flow is the consequence of a larger volume flow at the impeller exit resulting from the higher temperature.

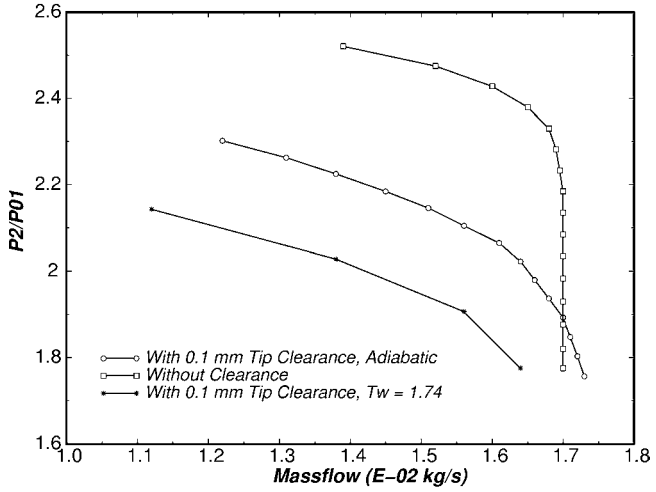

Figure 3 Impact of clearance and heat addition on static to total pressure ratio.

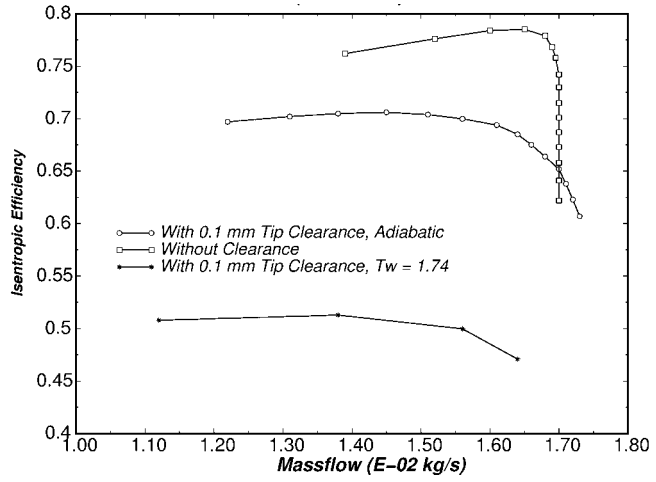

Figure 4 Impact of clearance and heat addition on total to total efficiency.

1D RADIAL COMPRESOR DESIGN.

The optimization of overall impeller dimensions (inlet and outlet radius, blade height and blade angle) requires a multipoint optimization of the impeller, diffuser and volute. The large number of flow analyses required prohibits the use of the expensive and time consuming Navier Stokes calculations.

The optimization of the compressor overall dimensions is made by the 1D design- and off design analysis program CCOD developed by Van den Braembussche (1990). The impeller flow calculation is based on the jet-wake model and is made in 2 steps:

- a first one calculates the flow from the leading edge to the point of flow separation (inducer part) . The location and velocity at separation is dependent on inlet geometry and maximum diffusion ratio (DR) at the shroud.
- a second one calculates separately the jet and wake flow and their mutual interaction, from the separation point to the trailing edge. The main parameter influencing the impeller exit conditions is the wake over jet velocity ratio (HNU).

After jet and wake mixing, downstream of the trailing edge, the program calculates the spanwise averaged flow in the diffuser by means of a skin friction coefficient according to Stanitz (1952). If applicable it continues with the calculation of the vaned diffuser of which the performance depends on the diffusion in the vaneless space and on the pressure rise in the divergent channel. Surge and stall limit are fixed, either by impeller incidence according to Rodgers (1962), vaneless diffuser limit flow angle according to Senoo and Kinoshita (1977) or maximum semi-vaneless space pressure rise according to Kenny (1972). The outcome are the mass flow, pressure ratio, efficiency and an estimation of operating range.

The starting version of this program assumes an adiabatic compression and the only heat addition is by disk friction . The new extended version calculates the flow conditions at separation point taking into account the temperature increase by the heat addition in the inducer. The temperature at the impeller exit accounts for the full impeller heat addition. It results in a lower density of the fluid and hence into a larger volume flow. It not only reduces the amount of separation but also the work input.

Two types of efficiencies are specified in the new version of the program:

- the first ones, η_{TT} and η_{TS} , are based on the inlet and outlet temperatures and hence decrease in proportion to the heat addition.
- the adiabatic total to total efficiency η_{AD} is based on the inlet and outlet total pressure and the different loss sources (incidence, separation, friction, mixing, clearance, disk-friction, etc.). It is not directly influenced by heat addition but takes into account the changes in flow path resulting from the larger volume flow.

Calibration of CCOD

As already mentioned, the 2D geometry of present design, with high pressure ratio and very large clearance, is quite different from the ones that have been used to define the correlations in the program CCOD. It has therefore been decided to recalibrate it by comparing the predictions with those obtained by a 3D Navier Stokes solver.

Calculations, similar to the ones shown on figure 3 and 4, have been made for different mass flows between choking and surge. The latter one is defined as the point where the Navier Stokes calculations fail to converge. The flow at the exit of the numerical domain is compared with the one predicted by CCOD at the same radius ratio.

The main empirical parameters, used to predict the flow in the impeller and that can be tuned to improve the agreement with experiments or calculations are the diffusion ratio ($DR=W_{LE}/W_{SEP}$) and the wake to jet velocity ratio ($HNU=W_W/W_J$).

Because of the non-optimum inlet geometry the diffusion ratio (DR) in the impeller had to be limited to 1.45. A detailed analysis of the flow predictions has also revealed that the present model, using a fixed value for HNU, is accurate only for moderate amounts of wake flow. The existing model showed some inaccuracies for the extreme cases where almost the whole exit section is filled with

wake because of the very large exit cross section.
The maximum diffusion ratio must be gradually decreased once the mass flow in the wake exceeds 40% of the total mass flow.
Once the mass flow in the wake is more than 90% of the total mass flow, the wake over jet velocity ratio is gradually decreased, starting at the standard value of .25. This was needed to avoid that all the mass flow would be in the wake. In that case there would be no jet and the model would no longer be able to predict the outlet static pressure. These corrections apply only for impellers with a too wide exit section because even at low wake/jet velocity ratio the wake mass flow is large because of the large section it occupies.
The impact of clearance on pressure rise and losses are verified by the results of figure 3 and 4
The results of the calculations with the new version of the CCOD program are compared to the Navier Stokes predictions on figures 5. The surge limit is rather well predicted (at least within the accuracy that can be expected for surge predictions by a Navier Stokes calculation)
The agreement is rather good for both operating conditions. The impact of 600 W heat transfer (non adiabatic calculations with 500 W in the impeller and 100 W in the short vaneless diffuser) is correctly predicted in terms of efficiency but the impact on pressure ratio is underestimated. One can conclude that the modified version of CCOD is sufficiently accurate to predict the performance of 2D high pressure ratio radial impellers. At the same time it is sufficiently fast to be used in the overall impeller dimension optimization procedure.
The prediction of the vaned diffuser performance has not been verified in more detail by a Navier Stokes solver because both the diffuser geometry and inlet flow conditions do not differ from the classical designs for which the method has been developed and

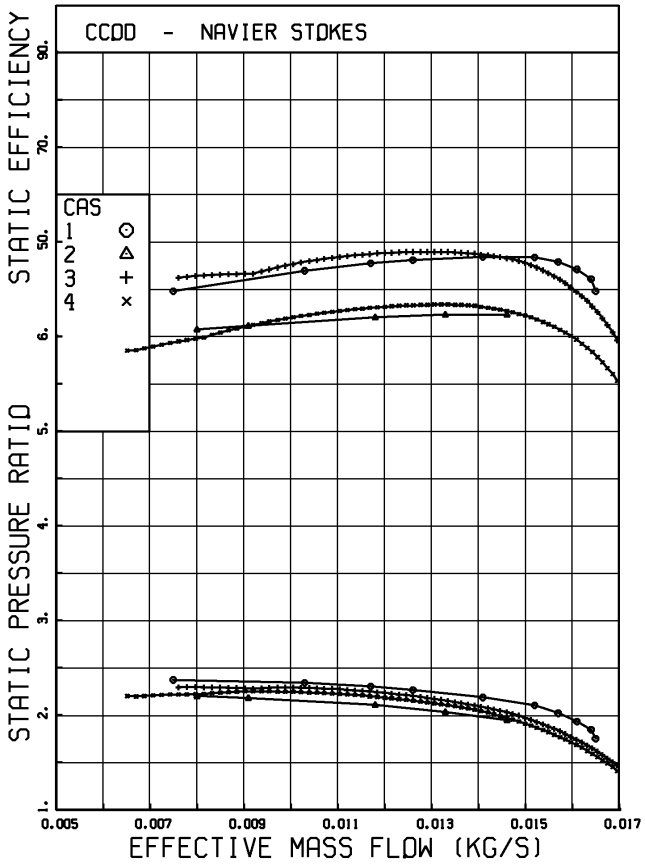

Figure 5 Comparison between CCOD and Navier Stokes predictions (⊕ Adiabatic Navier Stokes, Δ non-adiabatic Navier Stokes, + adiabatic CCOD, × non adiabatic CCOD)

calibrated previously. One can therefore conclude that this version of the program can also be used for the later optimization of the vaned diffuser.

Change of blade outlet angle.

Before continuing with a more detailed optimization of the impeller and the vaned diffuser one has first verified in how far the performance of present impeller geometry depends on the impeller outlet angle. This is done by analyzing the impact on pressure ratio and efficiency of a +- 10.^{o} change in blade exit angle. Results are listed in table 2

Table 2 impact of impeller outlet angle

β_{TE}		$\dot{m}$	π_{TT}	π_{TS}	η_{TT}	η_{TS}	η_{AD}
-50	adiab	0.0131	3.26	2.09	.685	.401	.681
	non adiab.		3.09	2.11	.531	.331	.671
-60	adiab	0.0131	2.93	2.07	.704	.454	.702
	non adiab		2.81	2.08	.531	.361	.695
-70	adiab	0.0131	2.63	2.04	.738	.523	.736
	non adiab		2.58	2.06	.541	.297	.737

One observes a small increase in total pressure ratio for more radial outward blades, however at the cost of a much lower efficiency. An increase of the blade exit angle from 60.0 ^{o} to 70.0 ^{o} results in a decrease of the outlet section perpendicular to the velocity, and thus in less diffusion and a smaller wake area. This possible gain in efficiency is annulled by larger friction losses in the longer blade channels. The combination of lower work input and higher friction losses results in a decrease of the total pressure ratio below the required value. One observes a small impact of the heat transfer on the adiabatic efficiency because of the change in flow pattern resulting from the higher temperature.
These comparisons indicate that an impeller outlet blade angle of 60.^{o} (that has been selected for this first 2D impeller study) should be close to the optimum value.

DETAILED IMPELLER OPTIMIZATION

The VKI optimization system is used for the detailed definition of the optimum impeller geometry. This design method is an extension to radial turbomachines by Cosentino et al. (2001) and Rini et al.(2001) of the approach developed by Pierret (1999) and Pierret et al. (1999). The basic idea of this method is a two-level optimization. A first one uses a rapid but less accurate analysis method by which a large number of geometries can be evaluated. It is followed by a more accurate but much more expensive Navier Stokes calculation to verify the optimum found in the previous step. The core of this knowledge-based design system (Fig. 6) is a **GENETIC ALGORITHM** in combination with an Artificial Neural Network (**ANN**) to **PREDICT** the performance of a given **GEOMETRY**. The **ANN** makes use of the knowledge acquired during previous designs of similar impellers and stored in a **DATABASE**.
Once the fast optimization loop is finished, the optimised geometry is verified by means of an accurate Navier-Stokes solver (**TRAF3D**) and the results of this calculation are added to the **DATABASE**. The cycle is stopped when the target **PERFORMANCE** is reached or when no further improvements are possible. In the other cases a new optimization loop is started after the **LEARNING** of the **ANN** on the new **DATABASE**. As the new **DATABASE** contains new information about impellers that are similar to the required one, one can expect that the next predictions by the **ANN** will be more accurate.
All computations have been performed on similar grids to guarantee a comparable accuracy for all the samples stored in the database. This is important because any erroneous information due to grid dependence, could drive the optimization process in a wrong direction.

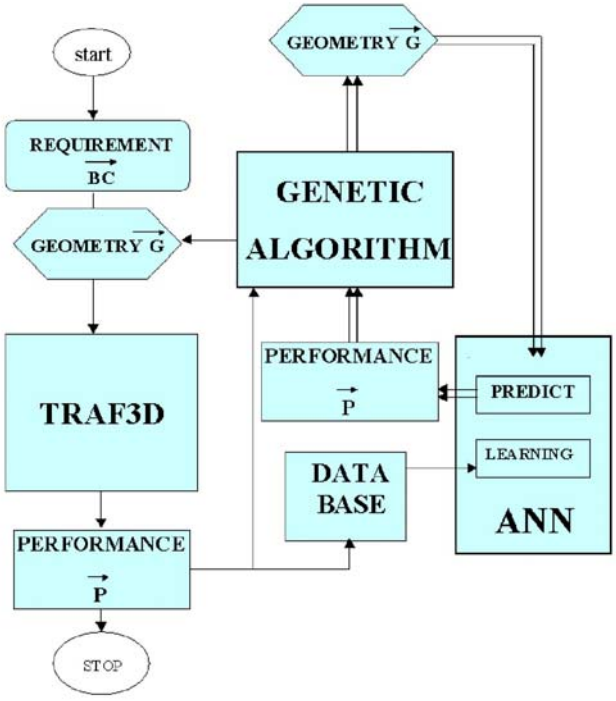

Figure 6 Flow chart of VKI optimization system

The Genetic Algorithm used in the present work is the one developed by David L. Carroll at University of Illinois and described in Yang et al. (1998). Typically 300 generations are created each containing 5 samples using the Micro Genetic Algorithm. Binary coding is used with the elitist tournament selection strategy. The algorithm allows uniform cross-over with a probability of 0.5 and a jump mutation with a probability of 0.02.

Artificial Neural Network

The multiplayer ANN have the powerful capability to be universal function approximators and once they are trained on an existing database they can be used to predict. The input and output are the same as the Navier Stokes solver. The ANN used in present study is the "SNNS" developed at the institute for Parallel and Distributed High Performance Systems of the University of Stuttgart. More information is given by Zoll et al. (1990). It has 7 nodes on the input layer (corresponding to the number of design variables), 16 nodes on the hidden layer, and 42 nodes on the output layer (mass flow, efficiency and Mach number in 20 points on pressure and suction side).

Geometry definition

The meridional contour, shown on figure 1, remains unchanged. Bezier curves are used to round off the inlet hub and shroud contour in order to create a more uniform flow at the impeller inlet and to facilitate the generation of the Navier Stokes grid. The hub contour, inclusive the parts upstream and downstream of the impeller can only shift in the axial direction as required by the condition of two-dimensionality. A first variable "b" defines the distance between the hub and shroud.

The blade camber line distribution from leading edge to trailing edge is defined by a third order Bezier curve written in Bernstein polynomial form in function of four additional variables β_0 to β_3.

$$\beta(u) = \beta_{LE}.(1-u)^3 + \beta_1 .u^2(1-u) \quad + \beta_2 .u(1-u)^2 + \beta_{TE}u^3$$

u is the non-dimensional length of the meridional contour (0 at the leading edge and 1 at the trailing edge).

The blade thickness is constant except near the leading edge where it is rounded off by an ellipse. A typical blade shape is shown on figure 2.

β_{TE} has a direct impact on pressure ratio and any change will result in a mass flow variation when the pressure ratio is imposed. In order to limit the deviations from the desired mass flow, the diameter R_{TE}. is systematically adjusted in function of the exit blade angle by means of following relation:

$$\Delta H_{\min,\max} = \omega\, R_{TE}\left[\omega\, R_{TE} - V_m .tg\beta_{TE\,\max,\min}\right]\sigma$$

The leading edge radius R_{LE} and the number of blades (NBL) are 2 additional design variables which brings the total on 7.

The clearance is .1 mm and kept constant during the optimization.

Objective function

The optimization of the compressor is driven by an objective function OF that decreases with increasing performance. It is the sum of three penalties: Depending on the application, the importance of each penalty can be modified by adjusting the respective weight factors w.

$$OF = w_{\dot m}.P_{\dot m} + w_\eta .P_\eta + w_M .P_M$$

The first penalty starts increasing when the calculated mass flow differs form the imposed one by more than 0.33%.

$$P_{\dot m} = \max\left[\frac{|\,\dot m_{req} - \dot m\,|}{\dot m_{req}} - \frac{\dot m_{req}}{300}, 0.0\right]$$

The second one increases with decreasing efficiency

$$P_\eta = \max(|\,\eta_{req} - \eta\,|,\ 0.0)$$

The penalty on the Mach number distribution aims for a smooth deceleration of the flow with minimum accelerations and with a margin for off design operation. It penalizes

- high peak values of the Mach number in the first half of the blade length, non dimensionalized by the average between inlet- and peak Mach number.

$$P_{M\,peak} = \max\left[\frac{M_{peak} - M_{in}}{M_{peak} + M_{in}}, 0.0\right]$$

- local reacceleration downstream of the Mach number peak

$$P_{M\,acc} = \sum_{i=i_{peak}}^{n} \max\left[\frac{M_i - M_{i-1}}{x_i - x_{i-1}}, 0.0\right]$$

- non uniform deceleration or acceleration

$$P_{M\,dec} = \max\left[\sum_{i=2}^{n} \left|\frac{dM_i}{dx_i} - \frac{dM_{i-1}}{dx_{i-1}}\right|, 0.0\right]$$

The Mach number penalties are applied separately for suction and pressure side. A weight factor is used to give more importance to the suction side where the risk of separation is larger.

Database

The initial database contains 11 samples (geometry, performance and Mach distribution calculated by the Navier Stokes solver). The geometries are generated by randomly perturbing the initial geometrical parameters within the limits defined by the feasible design space. 7 of those samples are used for the ANN training, 3 for the testing and 1 for validation. The learning is stopped when the predicted error for the test samples starts to increase. The learning sample is used to make a final check on how accurate the ANN can predict the performance of a geometry it has never seen before.

Convergence

The convergence of the optimization cycle is illustrated on figure 7 where the penalties predicted by the ANN are compared to those obtained from a Navier Stokes calculation. The changes proposed by the Genetic Algorithm are listed on table 3 together with the calculated mass flow and efficiency. The large discrepancies between Navier Stokes and ANN based penalties, observed during the first iterations, are mainly due to incorrect mass flow and non-optimum Mach number distribution. They indicate that the ANN predictions are not yet accurate and as a consequence the "optimum" geometry proposed by the Genetic Algorithm is not at all optimum. Based on these incorrect ANN predictions the Genetic Algorithm has proposed in iteration 7 a geometry it considers as optimum but which is not according to the Navier Stokes results.

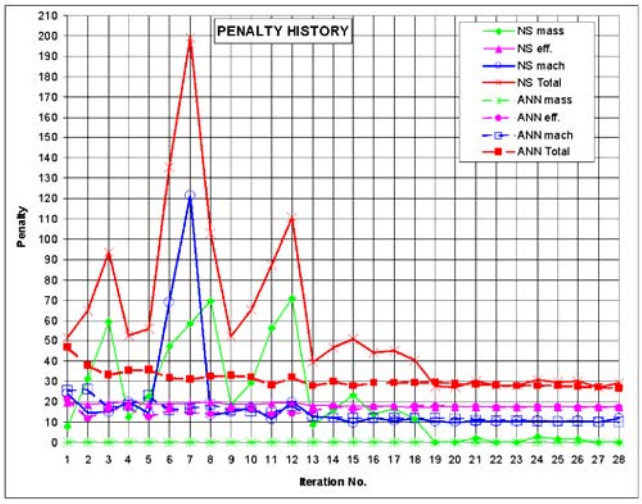

Figure 7 Convergence history (penalty versus iteration number)

Table 3

NO	b [mm]	$2R_{TE}$[mm]	β_0	β_1	β_2	β_3	NBL	$\dot{m}$ [gr/s]	η_{TT}
1	1.42	40.81	53.93	45.65	57.29	46.79	10	12.13	60.52
2	1.5	38.79	53.78	42.47	56.27	44.29	10	11.15	62.91
3	1.57	38.66	53.74	48.68	61.23	46.64	10	9.99	61.47
4	1.55	39.75	56.3	42.49	62.49	39.76	12	11.93	60.05
5	1.45	39.17	51.05	42.36	63.58	40.1	9	11.51	62.43
6	1.51	38.88	53	43.31	62.85	43.78	8	10.49	61.83
7	1.52	38.85	53.02	43.29	63.39	45.65	8	10.03	61.29
8	1.49	38.52	54.72	43.27	63.19	42.15	12	9.57	60.13
9	1.52	39.75	53.51	43.28	66	46.99	8	11.68	62.92
10	1.53	39.59	53.01	43.27	66	47.41	8	11.23	62.72
11	1.53	38.78	54.4	44.91	66	47.38	11	10.11	61.57
12	1.49	39.5	50.59	46.99	65.87	57.49	10	9.49	60.92
13	1.79	38.98	54.05	46.84	63.5	53.81	12	12.1	63.8
14	1.79	38.88	54.07	46.52	63.32	54.37	13	11.79	63.46
15	1.79	39.31	53.92	48.09	64.87	59.44	12	11.49	63.95
16	1.79	39.4	53.87	48.25	63.81	58.96	12	11.87	63.9
17	1.79	39.6	53.36	48.24	63.85	61.29	12	11.78	64.26
18	1.81	39.63	53.36	48.23	64.01	60.42	11	13.01	65.73
19	1.81	39.59	54.14	49.96	63.92	60.44	11	12.54	65.16
20	1.81	39.59	54.22	49.97	63.91	60.6	11	12.48	65.13
21	1.81	39.61	54.22	49.97	63.85	60.71	11	12.64	65.15
22	1.81	39.64	54.24	50.12	64.47	60.82	11	12.54	65.1
23	1.81	39.62	54.12	50.64	64.47	60.75	11	12.53	65.05
24	1.82	39.63	53.94	50.02	64.15	60.65	11	12.66	65.22
25	1.81	39.63	53.62	50.64	64.15	60.75	11	12.62	65.23
26	1.82	39.58	53.45	51.05	64.2	60.9	11	12.38	65.2
27	1.82	39.63	53.33	51.56	64.51	60.74	11	12.54	65.13
28	1.82	39.62	53	51.56	65.42	60.55	11	12.54	65.16

The discrepancy between the Mach number distribution predicted by the ANN and NS at iteration 7 is shown on figure 8. Although the ANN already predicts the main features of the Mach number distribution, there is still room for improvements.

Adding this geometry to the database and making a new learning results in a more accurate ANN. As a consequence the procedure becomes more accurate after each sample is added to the database and a new learning is performed. This self learning feature of the method is illustrated on figure 9 showing an almost perfect agreement between the Mach number predicted by Navier Stokes and ANN after 20 iterations. The difference in loading between figure 8 and 9 results from an increase of the vane number from 8 to 11 as indicated in table 3.

This figure also illustrates the kind of Mach distribution the Genetic Algorithm considers as optimum.

The total-to-total, adiabatic efficiency at iteration 20 is about 4 points higher than at the start of the optimization (table 3) and the Mach number distribution is clearly smoother and suggests a better off-design performance (Fig. 9).

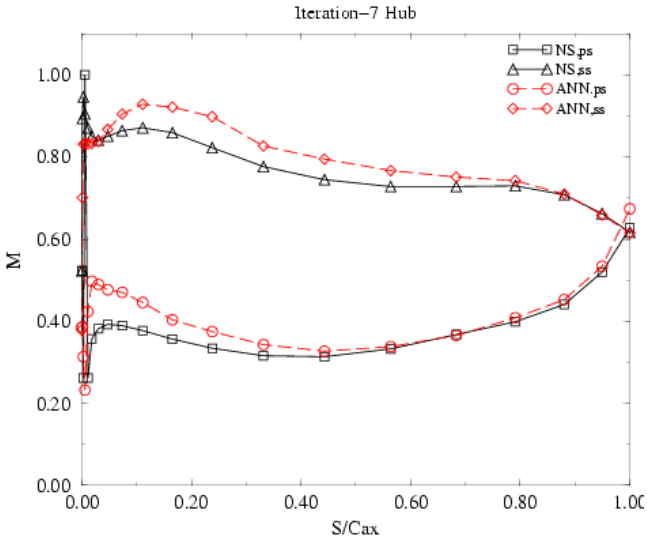

Figure 8. Comparison between ANN and NS predictions at iteration 7

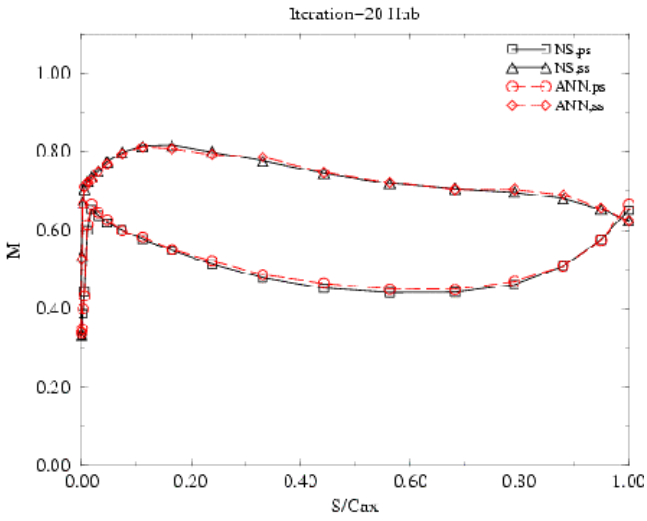

Figure 9. Comparison between ANN and NS prediction after 20 design iterations.

VANED DIFFUSER DESIGN

The last step in the compressor design is the definition of the vaned diffuser and volute.

The diffuser is of vaned island type. The main design parameters are the vane suction side angle (83.^{o}), the number of vanes (18), the total throat section (27.0 mm^2) and the diverging channel opening angle (12.^{o}) These values are the result of a systematic study by means of CCOD where efficiency and range are the main targets. The performance of the vaned diffuser is compared to the one with the vaneless diffuser on figure 10. One observes a large reduction in range and a considerable increase of the non-adiabatic efficiency. The volute is of collector type with large cross section.

SMALL SCALE COMPRESSOR PERFORMANCE

A final calculation has been made to find out how much the performance would change by a simple downscaling of the compressor by a factor 1/10 and operating it at the same peripheral speed. Assuming that this decrease of dimension and hence of Reynolds number from 50 000. to 5 000. would not alter the structure of the flow (from turbulent to laminar) this would provide the performance that is achievable with a button size gas turbine. The results of Navier Stokes calculations, with the same ratio of wall temperature as for the larger size, are compared to the adiabatic performance on figure 11.

One observes a non negligible decrease of pressure ratio and a nearly 10 points decrease of efficiency.

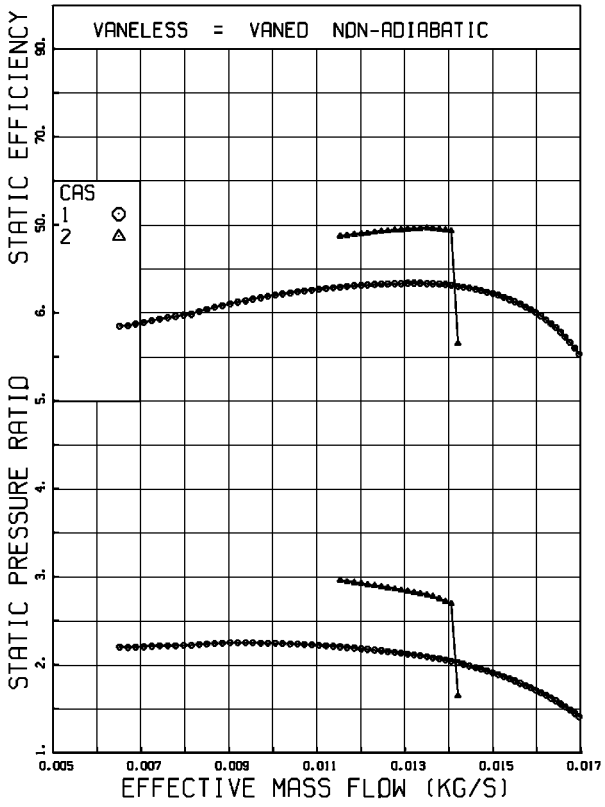

Figure 10. Performance of vaned and vaneless compressor

CONCLUSIONS

It has been shown that only small changes of the design and analysis methods, developed for high Reynolds numbers and near optimum specific speed, are needed to provide reliable results at the uncommon geometrical and operational conditions required by small gasturbines applications.

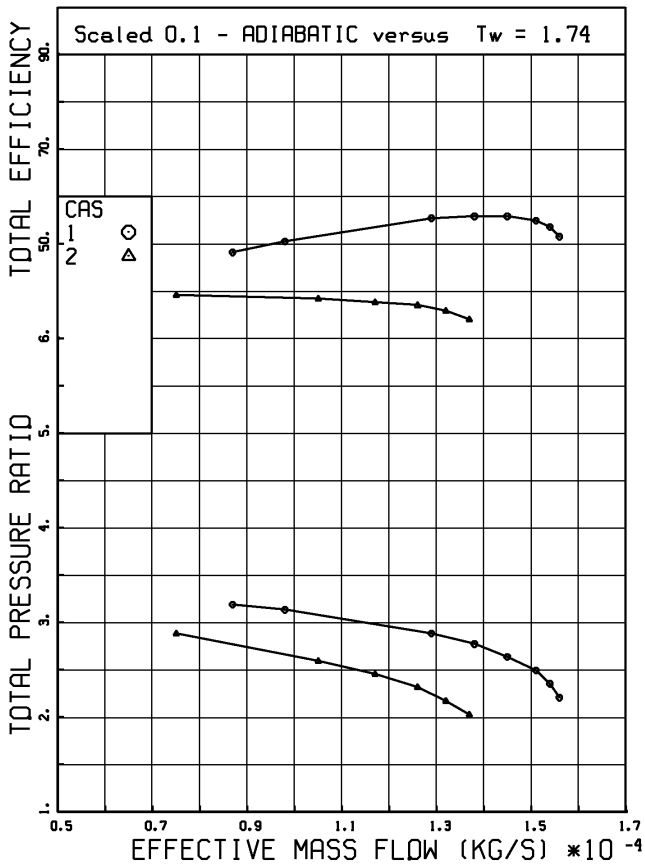

Figure 11. Performance of 1/10 scaled impeller – adiabatic ⊕ versus non-adiabatic Δ.

The impact of heat transfer on efficiency and pressure rise is studied and achievable performance is evaluated.

The expert system has shown to be a valuable tool for the optimization and detailed impeller design and allows reaching the required performance.

A Navier Stokes analysis of a 1/10 scaled down geometry provides an idea about the achievable performance of the small button size gasturbine compressor.

AKNOWLEDGEMENTS

This work was supported by "Development of Button-sized Gas GeneratorUtilization Technology" under FY2001 NEDO International Joint Research Project

BIBLIOGRAPHIC REFERENCES

Arnone, A., 1994, "Viscous Analysis of Three-Dimensional Rotor Flow Using a Multigrid Method", *ASME Journal of Turbomachinery*, Vol. 116, pp. 435-445.

Cosentino, R., Alsalihi Z,.and Van den Braembussche R.A., 2001, "Expert System for Radial Impeller Optimization", *Proceedings of the 4th European Conference on Turbomachinery*, Firenze, pp.481-490.

Kenny, D., 1972 " A Comparison of the Predicted and Measured Performance of High Pressure Ratio Centrifugal Compressor Diffusers", *VKI Lecture Series 50, Advance Radial Compressors*

Pierret, S., 1999, "Designing Turbomachinery Blades by Means of the Function Approximation Concept Based on Artificial Neural Network, Genetic Algorithm and the Navier-Stokes Equations", PhD Thesis, von Karman Institute,.

Pierret, S., and Van den Braembussche R.A., 1999, " Turbomachinery Blade Design Using a Navier Stokes Solver and Artificial Neural Networks", *ASME Journal of Turbomachinery*, Vol. 121, pp.326-332.

Ribaud Y., (2002), Private communication.

Rini, P., Alsalihi Z., and Van den Braembussche R.A., 2001, " Evaluation of a Design Method for Radial Impellers Based on Artificial Neural Network and Genetic Algorithm",. *Proceedings of the 5th ISAIF Conference*, Gdansk, pp. 535-543.

Rodgers, C., 1962, " Typical Performance Characteristics of Gasturbine Radial Compressors", *ASME Journal Engineering for Power*, Vol. 86, pp. 161-175.

Senoo, Y., and Kinoshita Y., 1977, "Influence of Inlet Flow Conditions and Geometries of Centrifugal Vaneless Diffusers on Critical Flow Angle for Reverse Flow", *ASME Journal of Fluids Engineering*, Vol. 99, pp.98-114.

Stanitz, J., 1952, "One Dimensional Compressible Flow in Vaneless Diffusers of Radial and Mixed Flow Compressors Including Effects of Friction, Heat Transfer and Area Change", NACA TN 2610.

Van den Braembussche R. A., 1990, "Design and Optimisation of Centrifugal Compressors, Course Note 141/TU, von Karman Institute,

Yang, G., Reinstein L.E., Pai S., Xu Z. and Carroll D.L.. 1998, "A New Genetic Algorithm Technology in Optimization of Permanent 125-1 Prostate Implants", Medical Physics.

Zell A., Korb, Th., Sommer, T., and Bayer R., 1990, "Applications of Neural Networks". *Conference Proceedings SPIE's Aerospace Sensing Intl. Symposium*, 1294, pp 16-20.